



Rational multiresolution analysis and fast wavelet transform: application to wavelet shrinkage denoising

A. Baussard^{a,*}, F. Nicolier^b, F. Truchetet^c

^aSATIE (UMR8029-CNRS/ENS/CNAM), 61 av. du Président Wilson, 94235 Cachan, France

^bLAM, 9 rue Québec, 10000 Troyes, France

^cLE2I (UMR5158-CNRS/UB), 12 rue de la fonderie, 71200 Le Creusot, France

Received 13 June 2002; received in revised form 19 May 2004

Abstract

This paper presents a contribution to rational multiresolution analysis (MRA). The rational analysis allows a better adaptation of scale factors to signal components than the dyadic one. The theory of rational MRA is reviewed and a pyramidal algorithm for fast rational orthogonal wavelet transform is proposed. Both, the analysis and synthesis parts of the process are detailed. Examples of scaling and wavelet functions and associated filters are given. Moreover, dealing with filters defined in Fourier domain, the implementation of the algorithm in this domain is described. Then, the study is extended to the 2D separable case in order to give a more conclusive presentation of the rational MRA.

In order to illustrate the potential of rational analysis for signal and image processing, some results given by wavelet shrinkage denoising based on the ‘SURE’ thresholding method are presented.

© 2004 Elsevier B.V. All rights reserved.

Keywords: Pyramidal algorithm; Rational multiresolution analysis; Rational wavelet transform; Wavelet shrinkage denoising

1. Introduction

Multiresolution analysis using the wavelet transform is an efficient way to span the information contained in a signal or an image. The dyadic MRA, corresponding to a scale factor equal to 2, was first introduced by Mallat [9]. In certain cases, this analysis is not fine enough to provide a good separation of signal components. The wavelet packets analysis can

be used but it does not generate embedded subspaces. Feauveau [7] proposed to refine the scale factor in his quincunx algorithm in the 2D case. In this analysis, two consecutive sublevels of decomposition are separated by a resolution factor of $\sqrt{2}$. An other way to increase the resolution of the analysis is to construct a rational extension of the filter banks theory [8]. Some relations have been established between this scheme and the wavelet transform. It appears that the rational filter banks cannot lead to true wavelet analysis [3,4].

Our work is inspired by the Ph.D studies of Auscher [1,2]. He has introduced a formal definition of rational MRA and a method to construct the associated orthogonal wavelet bases, but he gave no fast algorithm to compute the coefficients of the analysis. In practice, a

* Corresponding author. L2S (UMR8506-CNRS/SUPELEC/UPS), 3 rue Joliot Curie, Gif-sur-Yvette 91192, France.

E-mail addresses: baussard@lss.supelec.fr (A. Baussard), f.nicolier@iut-troyes.univ-reims.fr (F. Nicolier), f.truchetet@iutlecreusot.u-bourgogne.fr (F. Truchetet).

fast computation of wavelet transform implies that input signal is discrete. The computation is achieved in the dyadic case by the pyramidal algorithm proposed by Mallat [9]. In this contribution, the rational pyramidal algorithm which generalizes the Mallat algorithm and permits a better adaptation of the scale factor to signal is proposed. Some examples of orthogonal rational wavelet bases are provided as well as a practical implementation for fast computation. Moreover, a wavelet shrinkage denoising application, based on the Stein’s Unbiased Estimate of Risk (SURE) thresholding rules of Donoho and Johnstone [6], is presented.

The paper is organized as follows. A review of the MRA in the general case is presented in Section 2. Sections 3 and 4 present the rational pyramidal analysis and synthesis algorithm, respectively. Section 5 gives some implementation notes. Some rational wavelet bases are presented in Section 6 and the extension to the bi-dimensional case is introduced in Section 7. The wavelet shrinkage denoising application is presented in Section 8. Finally, Section 9 gives some conclusive remarks.

2. Rational multiresolution analysis

The rational MRA is formally defined by Auscher in [1] as a sequence of embedded subspaces V_j . This definition is a generalization of the MRA concept introduced by Mallat [9].

2.1. Approximation spaces

Theorem 1. Let M be a rational number ($M = p/q$, with $p, q \in \mathbb{Z}$ and $M > 1$). A sequence $\{V_j\}_{j \in \mathbb{Z}}$ of closed subspaces of $L^2(\mathbb{R})$ is a MRA of ratio M if the following properties are satisfied:

$$\forall j \in \mathbb{Z}, \quad V_{j+1} \subset V_j, \tag{1}$$

$$\overline{\bigcup_{j \in \mathbb{Z}} V_j} = L^2(\mathbb{R}), \tag{2}$$

$$\bigcap_{j \in \mathbb{Z}} V_j = \{0\}, \tag{3}$$

$$\forall j \in \mathbb{Z}, \quad f(x) \in V_j \Leftrightarrow f(M^{-1}x) \in V_{j+1}, \tag{4}$$

$$\forall k \in \mathbb{Z}, \quad f(x) \in V_0 \Leftrightarrow f(x - k) \in V_0. \tag{5}$$

An orthogonal basis of V_j is constructed by dilating and translating a mother function $\varphi(x) \in L^2(\mathbb{R})$, called the scale function. The basis functions of V_j are given by

$$\varphi_{j,n}(x) = M^{-j/2} \varphi(M^{-j}x - n), \quad j, n \in \mathbb{Z}. \tag{6}$$

Theorem 2. If in V_0 there exists a function φ such that $\{\varphi(x - k), k \in \mathbb{Z}\}$ is an orthogonal basis of V_0 , this function satisfies

$$\forall \omega \in \mathbb{R}, \quad \sum_{k \in \mathbb{Z}} |\widehat{\varphi}(\omega + 2k\pi)|^2 = 1, \tag{7}$$

$$|\widehat{\varphi}(0)| = 1, \tag{8}$$

$$\forall x \in \mathbb{R}, \quad \sum_{k \in \mathbb{Z}} |\widehat{\varphi}(x - k)| = \widehat{\varphi}(0). \tag{9}$$

The orthogonal projection of a function f over V_j can be considered as the action of a linear operator A_j on f :

$$A_j f = \sum_n \langle f, \varphi_{j,n} \rangle \varphi_{j,n} = \sum_n a_{j,n} \varphi_{j,n}. \tag{10}$$

2.2. Detail spaces

If the MRA conditions are satisfied, the MRA theory implies that there exist wavelet functions, noted ψ , which, with their dilation and translation, encode the information lost when approximating from one scale to a coarser one.

Theorem 3. W_j is defined as the orthogonal complement of V_j in V_{j-1} ($V_{j-1} = V_j \oplus W_j$) such that

$$f(x) \in W_j \Leftrightarrow f(M^{-1}x) \in W_{j+1}, \tag{11}$$

$$\forall j, k (\neq j) \in \mathbb{Z}, \quad W_j \perp W_k, \tag{12}$$

$$L^2(\mathbb{R}) = \bigoplus_{j \in \mathbb{Z}} W_j. \tag{13}$$

Then, the constructed subspaces W_j are embedded spaces.

Theorem 4. There exist $(p - q)$ wavelets $\psi^1, \dots, \psi^{p-q}$ in W_0 such that the set $\{\psi_{j,n}^m(x)\}_{j,n \in \mathbb{Z}, 1 \leq m \leq p-q}$ defines an orthonormal wavelet basis for $L^2(\mathbb{R})$.

So, there exist $(p - q)$ mother wavelets, each generating a subspace W_j^m (orthogonal to the others: $W_j^{n \neq m}$) included in V_{j-1} and the union of the W_j^m is the orthogonal complement of V_j in V_{j-1} :

$$V_{j-1} = V_j \oplus \bigcup_m W_j^m. \quad (14)$$

The basis functions are generated by the following equation:

$$\psi_{j,n}^m(x) = M^{-j/2} \psi^m(M^{-j}x - nq), \quad j, n \in Z. \quad (15)$$

The relation between $A_{j-1}f$ and $A_j f$ is given by $A_{j-1}f = A_j f + \sum_{m=1}^{p-q} D_j^m f$, where D_j^m is the projector over W_j^m . The projection of a function f over W_j^m is considered as the action of the linear operator D_j^m on f

$$D_j^m f = \sum_n \langle f, \psi_{j,n}^m \rangle \psi_{j,n}^m = \sum_n d_{j,n}^m \psi_{j,n}^m, \quad (16)$$

where $d_{j,n}^m$ are the detail coefficients.

3. Pyramidal analysis algorithm

In practice, the signal f is hardly available to carry out the analysis. The digital incoming signal is taken as the approximation at a given scale. Here, from an approximation (a_{j-1}) , the computation of the coarser approximation (a_j) and of the signal details (d_j^1) to (d_j^{p-q}) is described.

3.1. Approximation computation

As $V_0 \subset V_{-1}$, the decomposition of $\varphi(x - n) = \varphi_{0,-n}(x)$ in V_{-1} can be written

$$\varphi_{0,i}(x) = \sum_n h_i[n] \varphi_{-1,n}(x), \quad i = 0, \dots, q - 1, \quad (17)$$

where the q different sequences $h_i[n] = \langle \varphi_{0,i}, \varphi_{-1,n} \rangle$ can be considered as the impulse response of q numerical filters.

From Eq. (6), the scaling function can be written as

$$\varphi(x) = \sum_n h_i[n] M^{1/2} \varphi(Mx - Mi - n). \quad (18)$$

Then, the expression of $\varphi_{j,n}$ as function of $\varphi_{j-1,n}$ is obtained by inserting $\varphi(x)$ in (6):

$$\varphi_{j,n}(x) = \sum_k h_i[k] \varphi_{j-1, M(n-i)+k}(x) \quad (19)$$

with i such as $M(n - i) \in Z$.

The approximation coefficients are expressed from Eqs. (10) and (19):

$$a_{j,n} = \sum_k h_i[k] \langle f, \varphi_{j-1, M(n-i)+k} \rangle. \quad (20)$$

Let $r = M(n - i) + k$ and $\tilde{h}[n] = h[-n]$ the symmetric of h , it can be easily proved that

$$a_{j, sq+i} = \sum_r \tilde{h}_i[ps - r] a_{j-1, r} \quad (21)$$

with $s \in Z$ and $i = 0, \dots, q - 1$.

This equation shows that a_j is computed by convolving a_{j-1} with the filters $\{\tilde{h}_i\}_{0 \leq i \leq q-1}$ and keeping one sample out of p . The output of the downsamplers are delayed by i samples and q -upsampled (i.e, inserting $(q - 1)$ zeros between each sample of the signal). A final summation of the q signals leads to the coefficients a_j .

3.2. Detail computation

The decomposition of the wavelet functions $\psi^m(x)$, corresponding to the space $W_0 = \bigcup_{m=1}^{p-q} W_0^m$, over V_{-1} is given by

$$\psi^m(x) = \sum_k g_m[k] \varphi_{-1, k}(x) \quad (22)$$

which can be written as

$$\psi^m(x) = \sum_k g_m[k] M^{1/2} \varphi(Mx - k), \quad (23)$$

where $g_m[k] = \langle \psi_{0,0}^m, \varphi_{-1, k} \rangle$. Inserting (15) in (23) leads to

$$\psi_{j,n}^m(x) = \sum_k g_m[k] \varphi_{j-1, np+k}(x). \quad (24)$$

Let $r = np + k$, from Eq. (16), it can be proved that

$$d_{j,n}^m = \sum_r \tilde{g}_m[np - r] a_{j-1, r}. \quad (25)$$

This equation shows that the detail coefficients $d_{j,n}^m$ are computed by convolving a_{j-1} with the filter \tilde{g}_m and keeping one sample out of p .

The complete analysis algorithm is constructed from Eqs. (21) and (25). The structure of the algorithm is illustrated by the block diagram shown in Fig. 1.

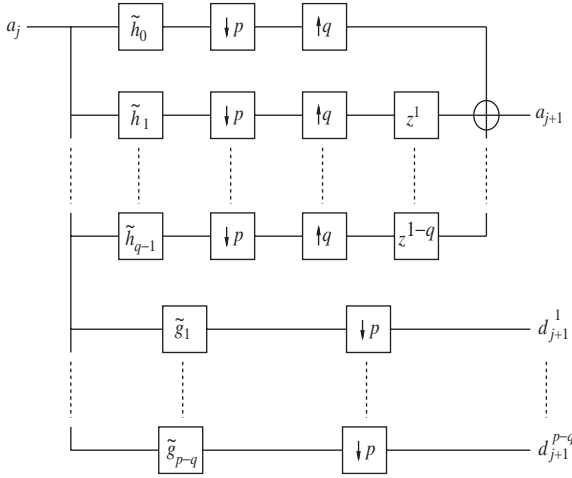


Fig. 1. Pyramidal analysis algorithm, decomposition of a discrete approximation a_{j-1} with a rational dilation factor $M = p/q$.

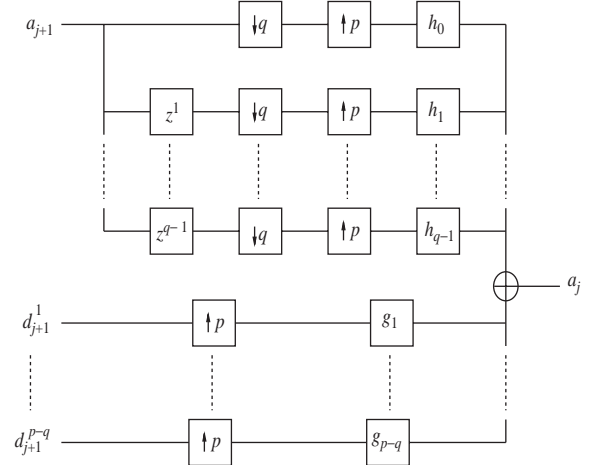


Fig. 2. Pyramidal synthesis algorithm, reconstruction of a discrete approximation a_j from the approximation coefficients a_{j+1} and the detail coefficients $d_{j+1}^1, \dots, d_{j+1}^{p-q}$.

4. Pyramidal synthesis algorithm

The synthesis algorithm is determined from the analysis equation

$$A_{j-1}f = \sum_n a_{j,n} \varphi_{j,n} + \sum_m \sum_n d_{j,n}^m \psi_{j,n}^m. \tag{26}$$

The signal coefficients are then reconstructed by summing two signals. From (10) and (16), one can write

$$a_{j-1,n} = \sum_k a_{j,k} \langle \varphi_{j,k}, \varphi_{j-1,n} \rangle + \sum_k \sum_m d_{j,k}^m \langle \psi_{j,k}^m, \varphi_{j-1,n} \rangle. \tag{27}$$

As $\varphi_{j,k}(x) = \sum_l h_l[l] \varphi_{j-1, M(n-i)+l}(x)$ and $\psi_{j,k}^m(x) = \sum_l g_m[l] \varphi_{j-1, n+lp+l}(x)$, this equation can be written as follows:

$$a_{j-1,n} = \sum_k a_{j,k} h_i[n - M(k - i)] + \sum_k \sum_m d_{j,k}^m g_m[n - kp]. \tag{28}$$

Eq. (28) shows that a_{j-1} is reconstructed by summing two signals. The structure of the corresponding algorithm is illustrated by the block diagram shown in Fig. 2.

One can note for the two proposed algorithms that for $M = 2$ the Mallat algorithm is recovered.

5. Implementation notes

5.1. Filter constructions

As the rational orthogonal wavelet bases are computed in Fourier domain (see Section 6), it is a good idea to construct the corresponding filters in this domain.

The impulse response coefficients of h filter are given by the following relation:

$$h_n[k] = \langle \varphi_{0,n}, \varphi_{-1,k} \rangle, \tag{29}$$

where $n = 0, \dots, q - 1$.

Using (6) and (19), it can be easily shown that these coefficients are computed, in Fourier domain, by

$$\hat{h}_n(\omega) = \sqrt{M} \frac{\hat{\varphi}(M\omega)}{\hat{\varphi}(\omega)} e^{-inM\omega}. \tag{30}$$

where i is the unitary imaginary number.

The impulse response coefficients of g filter are given by the following relation:

$$g_m[k] = \langle \psi_{0,0}^m, \varphi_{-1,k} \rangle, \tag{31}$$

where $m = 1, \dots, p - q$.

Using (15) and (24), these coefficients are computed, in Fourier domain, by

$$\hat{g}_m(\omega) = \sqrt{M} \frac{\hat{\psi}^m(M\omega)}{\hat{\varphi}(\omega)}. \tag{32}$$

5.2. Pyramidal algorithm implementation

In order to take advantage of these filters, defined in Fourier domain, it seems much more efficient to implement our pyramidal algorithm in this domain. Another point leading to this solution is that, as it is further shown, the filters involved are of infinite length so the implementation efficiency is far better in Fourier domain than in direct space.

In this subsection, we generalize a previous work [10] to the rational case.

5.2.1. Filtering and decay

In the proposed pyramidal analysis and synthesis algorithms, the filtering step, in Fourier domain, corresponds to a complex multiplication

$$a_n * h \rightarrow \hat{a}[k] \cdot \hat{h}[k]. \tag{33}$$

The decay z^p , in Fourier domain, corresponds to a phase displacement of $\exp(ip\omega)$.

5.2.2. Upsampling and downsampling

Following [10], let \hat{x}_n be the Discrete Fourier Transform (DFT) of the 1D signal x_k . This N samples signal is transformed into a pN samples signal \hat{y}_n with the following transformation:

$$\hat{y}_n = \hat{x}_{n \bmod N}. \tag{34}$$

Now, consider \hat{x}_n being the DFT of the 1D signal x_k . This N samples signal is transformed into a N/p samples signal \hat{y}_n with the following relation:

$$\hat{y}_n = \frac{1}{p} \sum_{l=0}^{p-1} \hat{x}_{pn+l}. \tag{35}$$

6. Rational wavelet bases

In [1] Auscher has proposed wavelet bases for rational MRA. The first one is an extension of the ‘Littlewood–Paley’ basis to the rational case. The other proposed bases are based on the Meyer construction. These ‘Auscher’ bases have been defined for $M = (q + 1)/q$ and $M = p/q$. They are closed to the ‘Littlewood–Paley’ basis but they allow better spatial resolution. In this contribution, the rational ‘Littlewood–Paley’ basis and the ‘Auscher’ Basis,

for $M = (q + 1)/q$, are reviewed and the corresponding filters allowing practical computation are given. These filters being linear in phase the corresponding wavelet transform are specially well suited for image processing.

6.1. Rational ‘Littlewood–Paley’ basis

The scale function of the rational ‘Littlewood–Paley’ basis is defined, in Fourier domain, by

$$|\hat{\phi}(M\omega)| = \begin{cases} 1 & \text{for } -q \frac{\pi}{p} \leq \omega < q \frac{\pi}{p}, \\ 0 & \text{elsewhere} \end{cases} \tag{36}$$

and the wavelet is defined by

$$|\hat{\psi}^m(M\omega)| = \begin{cases} 1 & \text{if } (q + m - 1) \frac{\pi}{p} \leq |\omega| < (q + m) \frac{\pi}{p}, \\ 0 & \text{elsewhere.} \end{cases} \tag{37}$$

The spectral bandwidth of the corresponding filters depends on the choice of p and q . Fig. 3 shows the magnitude of the scaling function and the wavelet in Fourier domain for $M = \frac{3}{2}$ and $M = \frac{5}{3}$. Fig. 4 shows the coefficients of the filters h_0, h_1 and g , corresponding to $M = \frac{3}{2}$ (filters taps amplitude decays as $1/n$).

6.2. ‘Auscher’ basis

The considered ‘Auscher’ basis has been defined for $M = p/q$ with $p = q + 1$. From [1], let $\chi(\omega)$ be an even and $C_\infty(R)$ function defined by

$$\begin{aligned} \chi(\omega) &= 0 & \text{if } \omega \in [0, a], \\ \chi(\omega) &= \frac{\pi}{4} + \beta(\omega - q\pi) & \text{if } \omega \in [a, b], \\ \chi(\omega) &= \frac{\pi}{2} & \text{if } \omega \in [b, Ma], \\ \chi(\omega) &= \frac{\pi}{4} - \beta\left(\frac{\omega}{M} - q\pi\right) & \text{if } \omega \in [Ma, Mb], \\ \chi(\omega) &= 0 & \text{if } \omega \in [Mb, +\infty[, \end{aligned} \tag{38}$$

where $a = (q - \varepsilon)\pi, b = (q + \varepsilon)\pi, \varepsilon \in]0, (1 + M)^{-1}[$ and β being an odd and $C_\infty(R)$ function such as

$$\forall \omega \in [\varepsilon\pi, +\infty[, \quad \beta(\omega) = \frac{\pi}{4}. \tag{39}$$

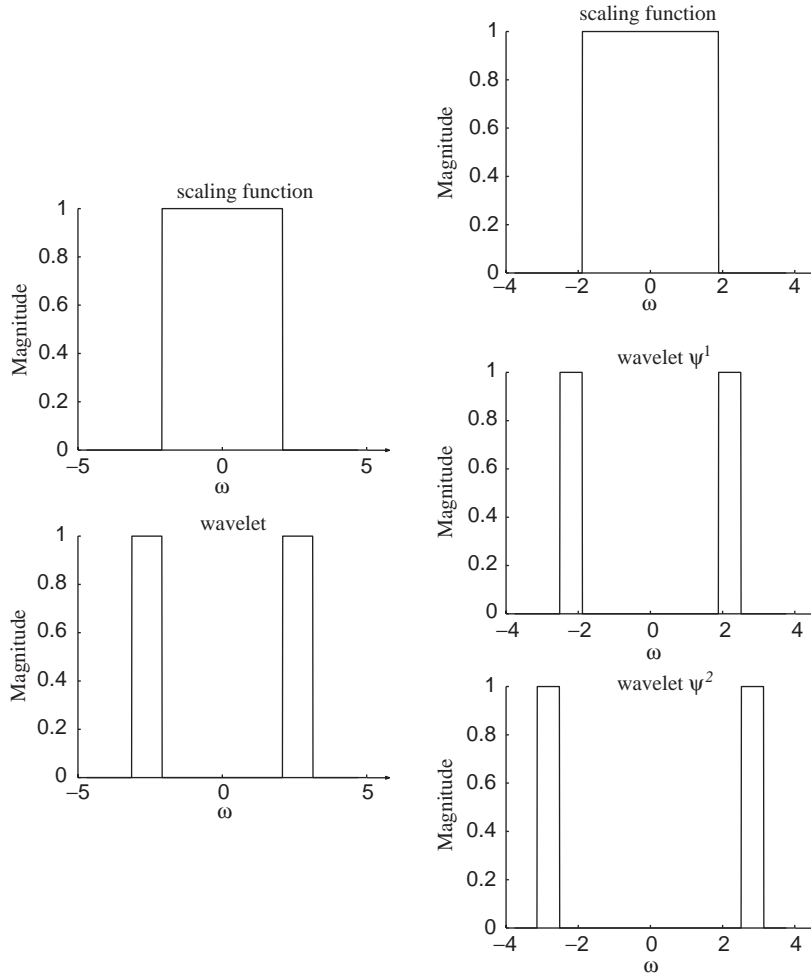


Fig. 3. Littlewood–Paley wavelet and scaling function for $M = \frac{3}{2}$ (left) and $\frac{5}{3}$ (right), in Fourier domain.

Then the scaling function is defined as

$$\hat{\phi}(\omega) = \begin{cases} \cos[\chi(\omega)] & \text{if } |\omega| \leq (q - \varepsilon)\pi, \\ 0 & \text{elsewhere} \end{cases} \quad (40)$$

and the wavelet by

$$\hat{\psi}(\omega) = \text{sign}_{q+1}(\omega) \sin[\chi(\omega)] \exp\left(-i \frac{\omega}{2}\right), \quad (41)$$

where $\text{sign}(\omega) = 1$ if $\omega > 0$ and -1 if $\omega < 0$.

In order to construct $\chi(\omega)$ within the intervals $[a, b]$ and $[Ma, Mb]$, we propose to use one of the following functions:

$$y = \frac{1 + \cos(x)}{2}, \quad (42)$$

$$y = 3x^2 - 2x^3, \quad (43)$$

$$y = 10x^3 - 15x^4 + 6x^5, \quad (44)$$

$$y = 35x^4 - 84x^5 + 70x^6 - 20x^7. \quad (45)$$

The three last functions permit to use different smoothness functions, zeroing various number of derivatives at end points and leading to faster decaying amplitude of filter taps.

Considering function (42) and $\varepsilon = (1 + M)^{-1}$, the scaling function and the wavelet in Fourier domain, for $M = 2$ and $\frac{3}{2}$ are presented in Fig. 5.

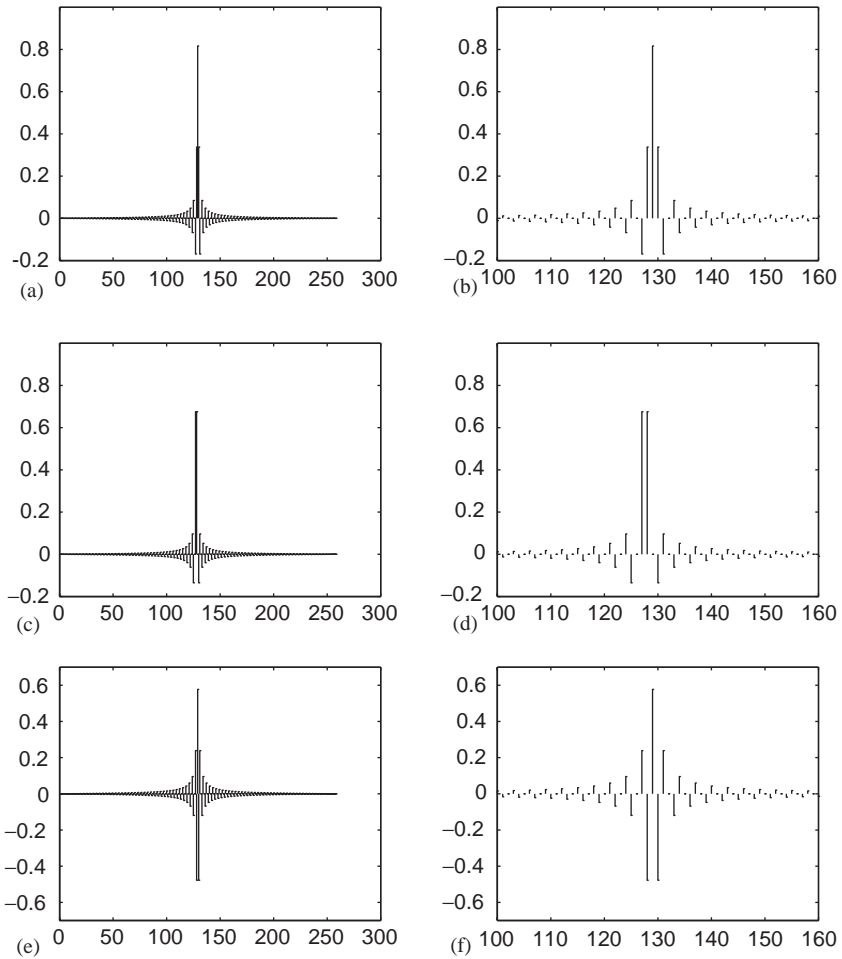


Fig. 4. Littlewood–Paley analysis for $M = \frac{3}{2}$: (a) filter coefficients h_0 . (c) Filter coefficients h_1 . (e) Filter coefficients g . (b), (d) and (f): zoom in the interest area of the filter.

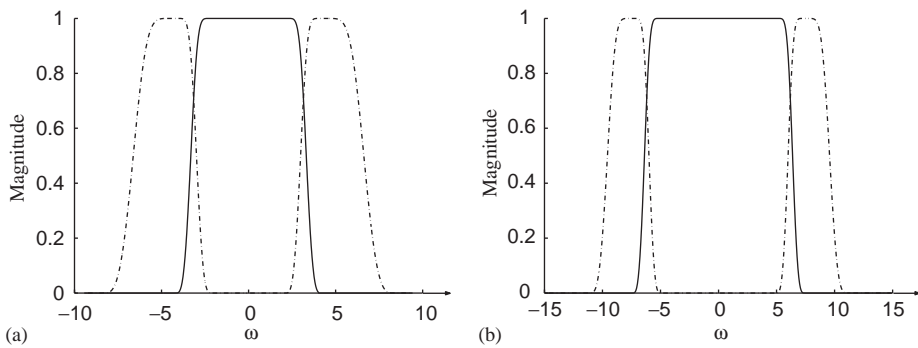


Fig. 5. Magnitude of the ‘Auscher’ scaling function (line) and wavelet (dashed line) for (a) $M = 2$ and (b) $\frac{3}{2}$, in Fourier domain.

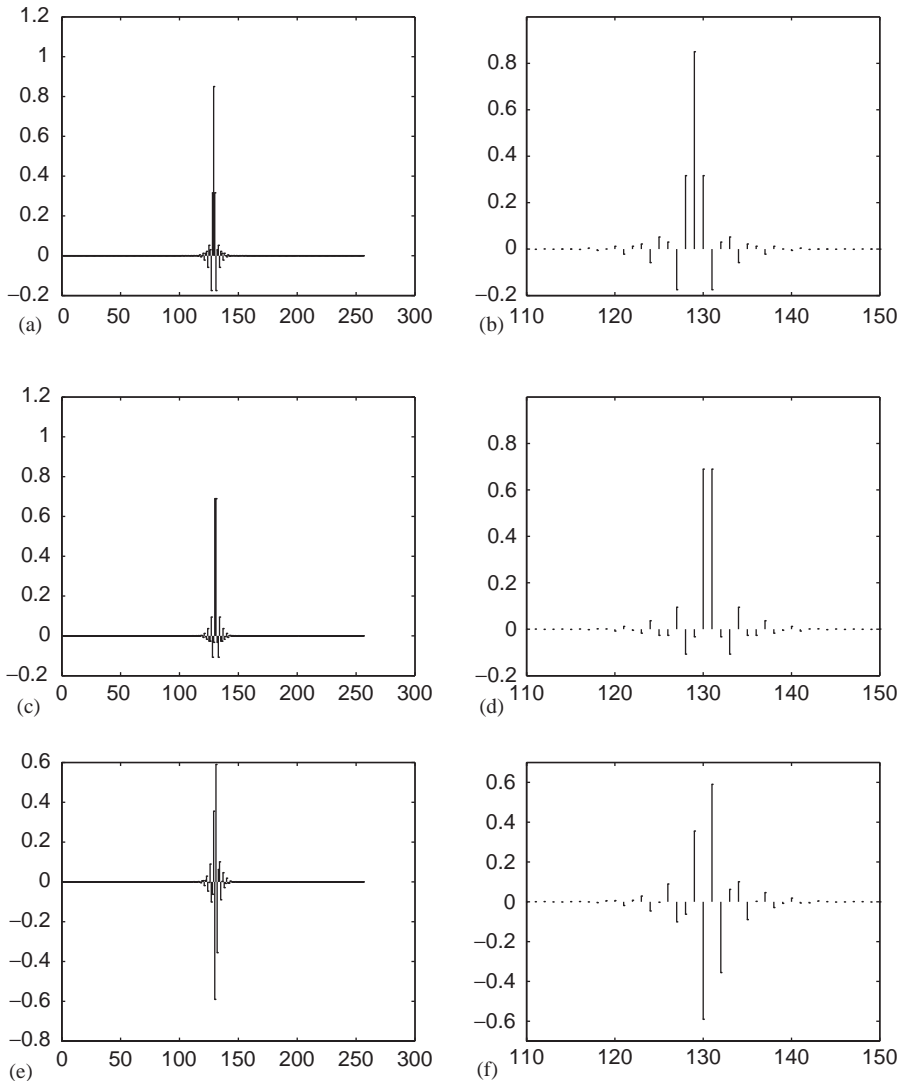


Fig. 6. ‘Auscher’ analysis for $M = \frac{3}{2}$: (a) filter coefficients h_0 . (c) Filter coefficients h_1 . (e) Filter coefficients g . (b), (d) and (f): zoom in the interest area of the corresponding filter.

In Fig. 6, the impulse response of the corresponding filters (h_0 , h_1 and g), obtained with the equations established in Section 5, for $M = \frac{3}{2}$ are shown.

These associated filters are with fast decaying infinite number of taps. The implementation in Fourier domain allows negligible discrepancy due to truncature.

7. 2D rational wavelet transform

As a more illustrative presentation, the rational decomposition of the ‘Lena’ image is presented in this section. The separable analysis case is considered with the ‘Littlewood–Paley’ basis. The analysis results, obtained for one scale, are shown for $M = 2$ (Fig. 7),



Fig. 7. Dyadic Littlewood–Paley wavelet transform.



Fig. 9. Littlewood–Paley wavelet transform for $M = \frac{5}{3}$.



Fig. 8. Littlewood–Paley wavelet transform for $M = \frac{3}{2}$.

$\frac{3}{2}$ (Fig. 8) and $\frac{5}{3}$ (Fig. 9). In these figures, one can notice the particular size of the resulting images.

In order to show the perfect reconstruction, the Peak Signal over Noise Ratio (PSNR) is computed. The PSNR is defined for a B bits gray level by

$$\text{PSNR} = 10 \log \left(\frac{(2^B - 1)^2}{d} \right) \text{ dB} \quad (46)$$

Table 1
PSNR results on the image obtained after one analysis and one reconstruction

M	2	$\frac{3}{2}$	$\frac{4}{3}$	$\frac{5}{3}$
PSNR (dB)	47.2	49.2	49.7	48.1

where d is the mean quadratic error given for a $[N_x \times N_y]$ image by

$$d = \frac{1}{N_x N_y} \sum_{i=0}^{N_x-1} \sum_{j=0}^{N_y-1} (I_0(i, j) - I_1(i, j))^2, \quad (47)$$

where I_0 is the initial image (without noise) and I_1 is the image to be compared.

Table 1 shows the PSNR results computed (with MATLAB[®] coding) after one analysis and one synthesis. The obtained results show that the considered basis and the proposed algorithm permit the perfect reconstruction of the decomposed signal (even with ‘longest’ filter).

8. Denoising by wavelet shrinkage

8.1. Wavelet shrinkage

In this contribution, in order to illustrate the potential of rational analysis, some results dealing with a signal and image denoising application are given. The

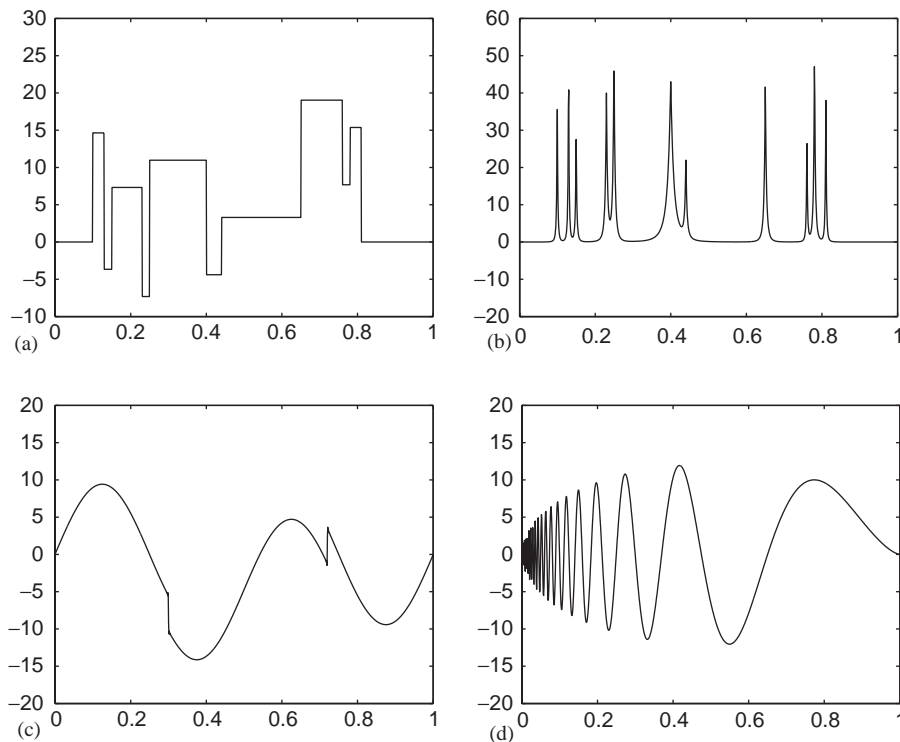


Fig. 10. (a) Signal 'Blocks'; (b) Signal 'Bumps'; (c) Signal 'HeaviSine'; (d) Signal 'Doppler'.

denoising method is based on wavelet shrinkage using the Stein's Unbiased Estimate of Risk (SURE) threshold selection [6,5]. The 'SURE' denoising method is based on an estimation of the noise variance. This estimation is obtained from the wavelet coefficients at first scale. Then the threshold computed from this estimation is applied at each scale in order to denoise the signal. One can note that this method, defined in the dyadic case, can be easily extended to our rational case.

In this application, for a better spatial resolution, the 'Auscher' bases defined for $M = (q + 1)/q$ are considered.

8.2. Signal denoising

In what follows, the considered signals (see Fig. 10) correspond to the ones proposed in [5]. In order to corrupt these signals, a gaussian noise, centered on high frequency, is added. Then, the previous denoising method, for $M = 2$ and $\frac{3}{2}$, is applied on

the four signals. To quantify the enhancement after denoising and to compare the results obtained using a dyadic and a rational analysis, the Signal to Noise Ratio (SNR) is computed.

Fig. 11 shows the high-frequency corrupted signals. Figs. 12 and 13 show the results after denoising for $M = 2$ and $\frac{3}{2}$, respectively, and Table 2 reviews the obtained SNR results. These results show that, for all signals, rational analysis leads to an improvement of the denoising process.

8.3. Image denoising

Taking into account the previous results, an image denoising application is presented. The 'Lena' image (see Fig. 14a), corrupted with a gaussian noise centered on high frequency (see Fig. 14b), is added. Fig. 14c and d show the results obtained with the 'SURE' method for $M = 2$ and $\frac{3}{2}$.

The PSNR, computed on the noised image, is equal to 22.85 dB. Table 3 gives results obtained after

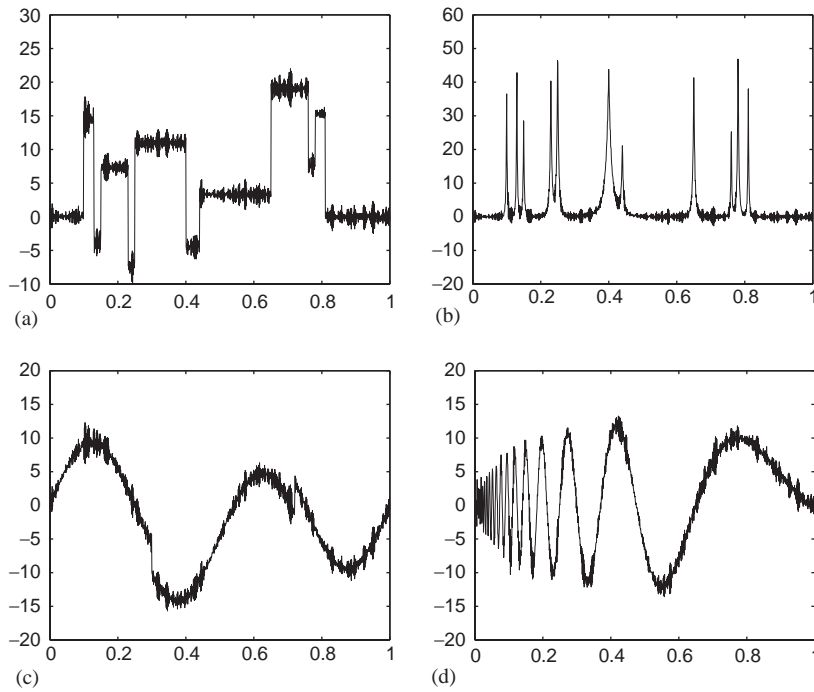


Fig. 11. Noised data with high frequency gaussian noise: (a) Noisy Blocks; (b) Noisy Bumps; (c) Noisy HeaviSine; (d) Noisy Doppler.

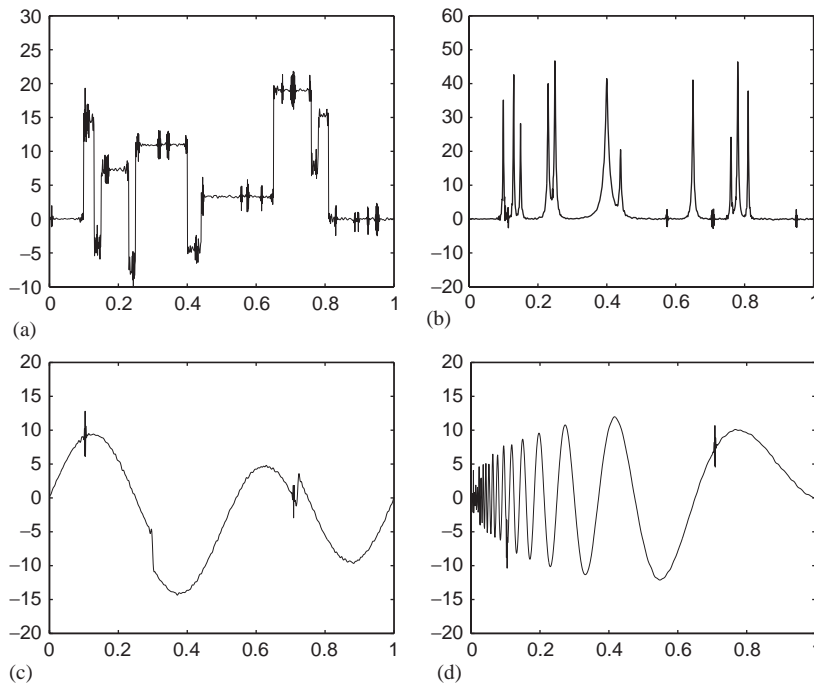


Fig. 12. Denoising results of the high-frequency corrupted signals for $M = 2$: (a) Signal 'Blocks'; (b) Signal 'Bumps'; (c) Signal 'HeaviSine'; (d) Signal 'Doppler'.

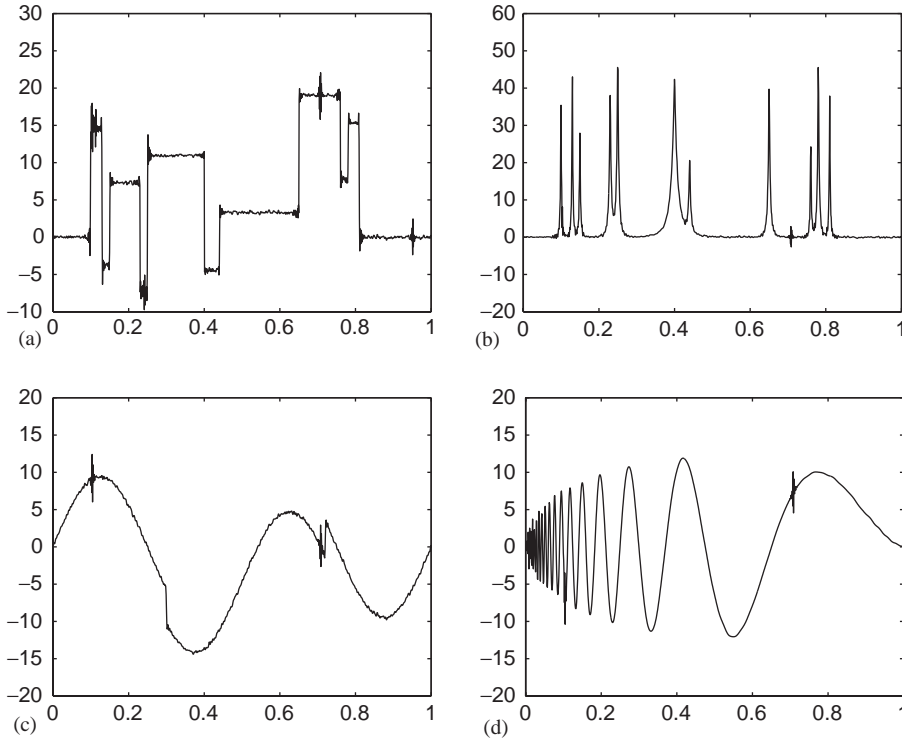


Fig. 13. Denoising results of the high-frequency corrupted signals for $M = \frac{3}{2}$: (a) Signal ‘Blocks’; (b) Signal ‘Bumps’; (c) Signal ‘HeaviSine’; (d) Signal ‘Doppler’.

Table 2
SNR (dB) results after denoising for the high frequency gaussian corrupted signals

	Blocks	Bumps	HeaviSine	Doppler
Initial	17.77	16.28	15.91	15.70
$M = 2$	21.11	22.91	28.56	25.93
$M = \frac{3}{2}$	24.29	24.03	28.76	28.67

denoising by the dyadic and the rational analysis using the ‘Auscher’ bases. Once again, these results show an improvement of the denoising process when using rational analysis instead of classical dyadic one.

9. Conclusion

In this paper, rational orthogonal MRA which extends the potentialities of dyadic MRA has been presented. This analysis provides a better adaptation of the scale factor to the signal information. Some examples of rational MRA and the construction of



Fig. 14. (a) ‘Lena’ image. (b) Noised image. (c) Denoised image with $M = 2$. (d) Denoised image with $M = \frac{3}{2}$.

associated filters for rational orthogonal MRA have been proposed. A pyramidal algorithm for the computation of rational MRA coefficients has been pre-

Table 3
PSNR (dB) results obtained for the image denoising

M	2	$\frac{3}{2}$
PSNR	26.51	27.97

sented. Both analysis and synthesis parts of the process have been detailed for one-dimensional signals. Moreover Fourier domain implementation has been described. In order to give a more illustrative presentation of rational MRA, examples of two-dimensional decompositions, in the separable case, have been presented. An application to wavelet shrinkage denoising has been proposed in order to show the potential of rational MRA. These results are only preliminary elements for a more complete study of rational wavelet shrinkage algorithms, still to be done. Moreover, rational MRA could be interesting in other applications like fractal analysis, signal characterization or even feature extraction and pattern recognition in image processing.

Further researches will lead to new basis functions with better spatial and temporal features and to non-separable multidimensional pyramidal algorithm.

References

- [1] P. Auscher, *Ondelettes fractales et applications*, Ph.D. Thesis, Dauphine University, Paris IX, France, 1989.
- [2] P. Auscher, Wavelet bases for $L^2(R)$ with rational dilation factor, in: M.B. Ruskai et al. (Eds.), *Wavelets and their Applications*, Jones and Barlett, Boston, 1992, pp. 439–452.
- [3] T. Blu, Iterated filter banks with rational rate changes—connections with discrete wavelet transform, *IEEE Trans. on Signal Process.* 41 (June 1993) 3232–3244.
- [4] T. Blu, A new design algorithm for two-band orthonormal rational filter banks and orthonormal rational wavelets, *IEEE Trans. on Signal Process.* 46 (June 1998) 1494–1504.
- [5] R. Coifman, D. Donoho, Time-invariant wavelet denoising, in: A. Antoniadis, G. Oppenheim, *Lecture Notes in Statistics*, Vol. 103, Springer, Berlin, 1995, pp. 125–150.
- [6] D. Donoho, I. Johnstone, Adapting to unknown smoothness via wavelet shrinkage, *J. Amer. Statist. Assoc.* 90 (December 1995) 1200–1244.
- [7] J.-C. Feauveau, Analyse multiresolution avec un facteur de résolution $\sqrt{2}$, *J. Traitement du Signal* 7 (2) (1990) 117–128.
- [8] J. Kovačević, M. Vetterli, Perfect reconstruction filter banks with rational sampling factors, *IEEE Trans. Signal Process.* 41 (June 1993) 2047–2066.
- [9] S. Mallat, A theory for multiresolution signal decomposition: the wavelet representation, *IEEE Trans. Pattern Anal. Machine Intell.* 11 (July 1989) 674–693.
- [10] F. Nicolier, O. Laligant, F. Truchetet, Discrete wavelet transform implementation in Fourier domain, *J. Electron. Imaging* 11 (2) (July 2002) 338–346.